S.M. Adler-Golden, S. Richtsmeier, P. Conforti and L. Bernstein, Spectral Image Destriping using a Low-dimensional Model, Proc. Proc. SPIE 8743, Algorithms and Technologies for Multispectral, Hyperspectral, and Ultraspectral Imagery XIX, 87431Q, (2013).

doi:10.1117/12.2014317

See next page.

Spectral image destriping using a low-dimensional model

S. Adler-Golden*, S. Richtsmeier, P. Conforti and L. Bernstein
Spectral Sciences, Inc., 4 Fourth Avenue, Burlington, MA 01803-3304

ABSTRACT

Striping effects, i.e., artifacts that vary systematically with the image column or row, may arise in hyperspectral or multispectral imagery from a variety of sources. One potential source of striping is a physical effect inherent in the measurement, such as a variation in viewing geometry or illumination across the image. More common sources are instrumental artifacts, such as a variation in spectral resolution, wavelength calibration or radiometric calibration, which can result from imperfect corrections for spectral "smile" or detector array nonuniformity. This paper describes a general method of suppressing striping effects in spectral imagery by referencing the image to a spectrally low-dimensional model. The destriping transform for a given column or row is taken to be affine, i.e., specified by a gain and offset. The image cube model is derived from a subset of spectral bands or principal components thereof. The general approach is effective for all types of striping, including broad or narrow, sharp or graduated, and is applicable to radiance data at all optical wavelengths and to reflectance data in the solar (visible through short-wave infrared) wavelength region. Some specific implementations are described, including a method for suppressing effects of viewing angle variation in VNIR-SWIR imagery.

Keywords: Hyperspectral, multispectral, image, striping, destriping, spectral smile

1. INTRODUCTION

Striping artifacts, i.e., intensity variations that are functions of the column or row of an image, may be caused by a variety of effects involving the sensor or viewing conditions. In multispectral and hyperspectral imagery, the stripes may be oriented along either the along-track (scan) direction or the cross-track direction. Wavelength calibration variation, such as inaccurately compensated spectral "smile", can interact with narrow atmospheric absorption features to produce along-track striping that is typically broad and smooth. More common is along-track striping caused by drift in the radiometric responses of detector array elements or problems in the readout electronics. An example of such striping in the blue region of NASA's Hyperion sensor is shown in Figure 1. The striping here includes a periodic pattern, some broad banding, and single-pixel stripes from individual detector elements

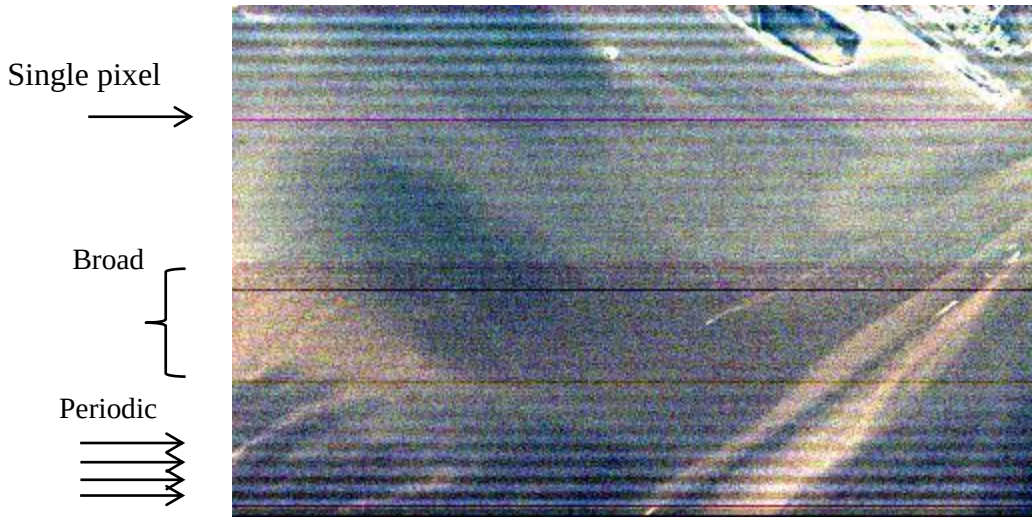

Figure 1. Striping in a false color Hyperion image of Galveston Bay. RGB = (468, 447, 427) nm, ENVI "2% linear" rendering. The image is rotated so that the scan direction is from left to right.

*adlergolden@spectral.com; phone 1 781 273-4770; fax 1 781 270-1161; spectral.com

Another potential source of intensity variation across an image is a wide angular field of view. Here different line of sight (LOS) geometries at different positions in the image can generate a smooth, graduated "striping" associated with the varying scattering angle and length of the air column. The effect is noticeable in some imagery from the JPL AVIRIS sensor, which has a 30 deg cross track field of view. It is most pronounced with off-nadir viewing, as illustrated by a hyperspectral image simulation from the MCScene code[1], shown in Figure 2. Here the increased atmospheric path length at the top of the image results in enhanced haze effects (increased brightness and reduced contrast).

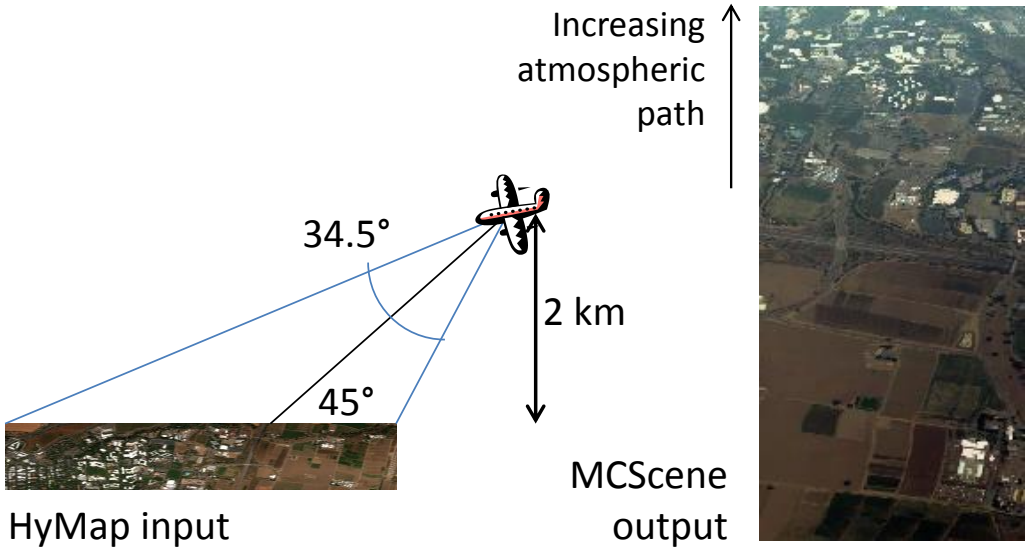

Figure 2. Atmospheric "striping" in a simulated wide-angle hyperspectral image of Davis, CA (image is displayed with ENVI "2% linear" rendering).

First-principles compensation for striping can be challenging, as it needs to be adapted to the sensor system characteristics and the specific phenomenology that causes it. A simpler and more versatile approach is to use an empirical, in-scene destriping method. The literature on such methods is vast; a recent review is given by Carfantan and Idier.[2] A very basic method is to match the mean or integrated intensities in the striping direction (i.e., down the columns or rows) to the same value.[3] This is done most simply by applying either gain factors or offsets. One can also derive both gains and offsets for destriping by matching multiple moments of the data, such as means and standard deviations. The implicit assumption is that the signal statistics within all column or rows should be equivalent. This assumption is reasonable when the scene clutter is low and/or on a fine spatial scale and the image is sufficiently large, but it breaks down with small images, strong scene contrasts, and clutter scales comparable to the image dimensions. A generally better method is to normalize the data to locally smoothed statistics, such as running average integrated intensities.[4] This method is robust to clutter effects and effectively suppresses narrow striping; however, it is ineffective for the broad, smooth striping arising from spectral smile or viewing angle variation. With hyperspectral imagery, which may contain groups of bands with similar statistics, moment matching or normalization can be performed within these groups.[5]

This paper describes a simple, versatile and computationally fast destriping approach for hyperspectral and multispectral imagery that leverages the multiplicity of spectral bands but does not require statistics matching across either bands or spatial regions. The basic idea is that the number of bands exceeds the spectral dimensionality (number of linearly independent components) needed to model the full image well enough for deriving an affine destriping transform (i.e., a transform containing both gains and offsets). The approach assumes the existence of multiple linearly independent bands that are free of striping either individually or collectively (i.e., in averages or other combinations). The unstriped "reference" images are used to build an unstriped low-dimensional model, typically between 2 and 6 dimensions, that represents all bands of the image. The model is then used to derive the destriping transform via linear regression. No assumptions are required about the spatial properties of the striping, and no spatial convolutions, transforms or other types of spatial filtering are used. In our work to date the approach has proved very effective for many different types of striping, including broad or narrow, sharp or graduated, and it is applicable to all optical wavelengths. We illustrate the approach using the Figure 1 and Figure 2 cases.

1.1 General algorithm description

Consider a three-dimensional spectral image given by intensities Y_{ijk}, where i is the pixel index along the stripe direction, j is the pixel index perpendicular to the stripe direction, and k is the wavelength band index. The image is presumed to contain unstriped bands, which are taken individually or in linear combinations to form N (1 or greater) linearly independent unstriped "reference" images, denoted X_{ijl}, where l is the image index between 1 and N. Then we write an N-dimensional, unstriped approximation to the original data Y_{ijk} as a linear combination of the reference images, with k-dependent fitting coefficients denoted A_{kl} plus a constant term A_{k0}. That is, the N-dimensional model for band k is given by

$$M_{ijk} = \Sigma_l A_{kl} X_{ijl} + A_{k0} = Y_{ijk} + \text{error} \quad (1)$$

The fit parameters A_{kl} and A_{k0} are determined by least squares error minimization. If one portion of the image is known to have higher fidelity than the rest (for example, if it has a more accurate spectral or radiometric calibration) and contains representative scene content, it is sensible to derive the parameters from that portion alone; otherwise, the entire image is used in the fit.

The N-dimensional model is then used to derive a destriping transform for all of the bands. This is done by applying a linear regression analysis to each row or column along the stripe direction to determine j- and k-dependent offset and gain coefficients, B_{jk} and C_{jk}, that best fit the model to the data. That is,

$$M_{ijk} + \text{error} = B_{jk} + C_{jk}\, Y_{ijk} \quad (2)$$

The right-hand side of (2) is the regression fit and constitutes the destriped data Z_{ijk}:

$$Z_{ijk} = B_{jk} + C_{jk}\, Y_{ijk} \quad (3)$$

The destriping transform is thus defined by the spatially and spectrally dependent gain terms C_{jk} and offset terms B_{jk}.

The spectral dimensionality of the destriped data equals that of the original data, regardless of the size of N, but the N value does affect the results. In particular, too many reference images (too large an N value) may allow subtle striping present in those images to emerge in the model in amplified form, thus making the destriping algorithm ineffective. To date we have obtained good results with N between 2 and 6. When there are more than this number of unstriped bands in the data, we may perform a principal component analysis on the unstriped bands and take N leading principal component images, which are linear combinations of the bands, as the references.

1.2 Application to the Hyperion visible-near infrared (VNIR) spectrometer

The Hyperion image in Figure 1 has close to 50 bands of valid radiance data from the VNIR spectrometer at wavelengths between 427 and 925 nm. Striping is very pronounced at the shortest wavelengths and decreases gradually with increasing wavelength. We considered the 20 bands from 711 nm to 905 nm as unstriped, constructed and diagonalized their covariance matrix, and from the leading eigenvectors derived principal component images for use as reference bands. Hyperion also provides short-wave infrared coverage with a second spectrometer, and ordinarily we would incorporate that spectral region in the reference bands to improve the fidelity of the model. However, we did not do so here because the two spectrometers are slightly spatially misaligned.

The destriped result for N=4 is shown in Figure 3. Visual inspection indicates that the striping is almost completely removed; only tiny amounts remain near the top and bottom edges.

For a closer look at the result, Figure 4 shows the integrated intensities along the striping direction (column sums) at four different visible wavelengths, corresponding to three striped bands and one unstriped band. The destriped results (colored curves) eliminate the periodic pattern and the single-column spikes, including a spike in the nominally unstriped 732 nm band (blue curve). Unlike a simple normalization-based destriping, which would equalize the column sums, the current scheme does a good job of preserving the cross-track brightness trends associated with the various terrain types, which in this image include clear water, foam, and land surfaces.

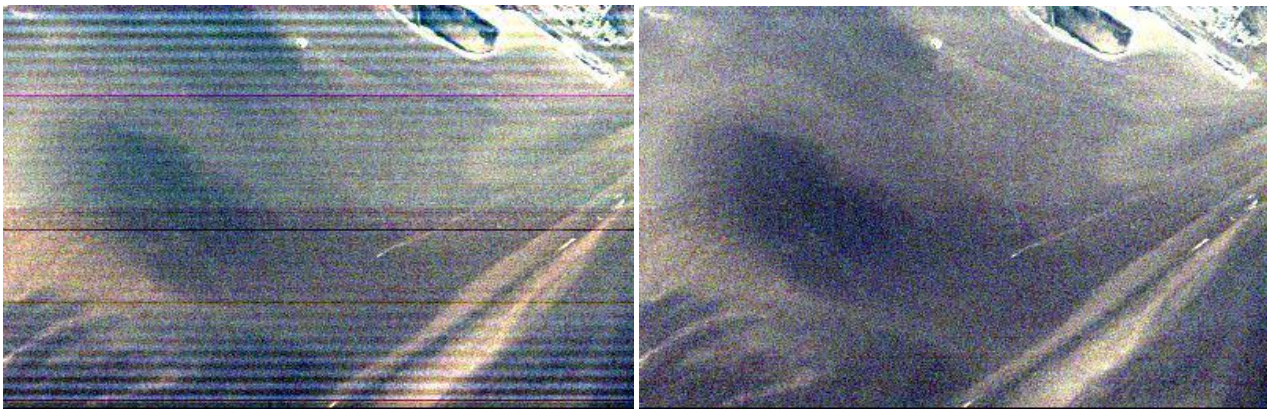

Figure 3. Hyperion image before (left) and after (right) destriping.

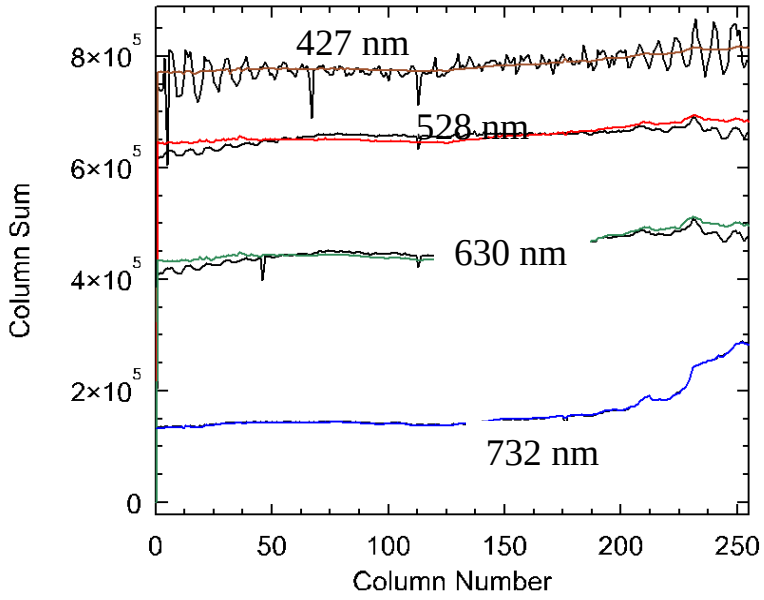

Figure 4. Comparisons of original integrated column intensities (rough traces) with results after destriping (smooth traces).

1.3 Variant of method for destriping wide-angle VNIR-SWIR imagery

We now consider the challenging case of viewing the earth in the visible through near- and short-wave infrared (VNIR-SWIR) region with a wide, off-nadir angular field of view from several km altitude or greater. The images may be in either radiance units or what we call "nominal" reflectance units—i.e., the output from a standard atmospheric correction or "compensation" algorithm that assumes a fixed viewing geometry. These algorithms include the popular Empirical Line Method (ELM)[6], the Quick Atmospheric Correction (QUAC)[7], and first-principles algorithms such as FLAASH®.[8] Here the image contains "striping" associated with the viewing angle variation in both atmospheric absorption and scattering, which occurs primarily at visible wavelengths. The scattering includes both backscattering and forward scattering components; the latter, known as the adjacency component, involves locally averaged surface-leaving radiance.

In our destriping transform the spatial variation in atmospheric scattering is compensated by the spatially varying, spectrally dependent offset, while the spatial variation in atmospheric absorption is compensated by the spatially varying, spectrally dependent gain. This is analogous to the ELM and QUAC assumption that the effects of a uniform atmosphere can be compensated with uniform gains and offsets. This assumption is rigorous for all atmospheric effects except adjacency scattering.

As IR wavelengths are relatively free of atmospheric scattering effects, they are potentially a good source for reference bands. However, because they are insensitive to green vegetation they have limited ability to model the full range of terrain at visible wavelengths. To get around this problem we derive the destriping transform using only non-vegetated pixels. This has the drawback of limiting the ability to derive offsets, which are best obtained from dark pixels such as vegetation. Accordingly, we have modified our destriping procedure to use a multi-step approach, in which the visible offsets are derived from dark pixels, and then the visible gains are determined from bright, non-vegetated pixels using a low-dimensional model. In addition, rather than simply preserving the IR bands in the original data, we add a final step in which (3) IR gains and offsets are estimated by extrapolating from the visible using simple scattering assumptions. The detailed procedure, starting from a nominally atmospherically corrected image, is as follows:

Visible B_{jk} (offset) determination:

- The image is divided into strips (of order 10) of similar view angle (i.e., along the strip direction);
- Dark pixels (reflectance < ~0.05 at 2 μm) are selected by thresholding the reflectance at 2 μm;
- The visible band minima are found in each strip containing at least a few (~4) dark pixels;
- The minima for each band k are fit to a parabola or other smooth function of j, defining the visible offset.

Visible C_{jk} (gain) determination:

- Bright pixels (reflectance > ~0.35 at 2 μm) are identified in the scene;
- Eq. (1) is used to build a best-fit visible model for the bright pixels; 3 to 6 IR bands in atmospheric window regions are used as the references;
- The model estimates M_{ijk} are calculated for the bright pixels;
- Using the previously determined B_{jk} and the model estimates, Eq. (2) is applied to each strip that has a minimum fraction of bright pixels; the fit results define the visible gains for those strips;
- The gains for each band are fit to a smooth function of j, thus defining C_{jk} in the visible region.

IR offsets and gains:

- The visible gain inverse is identified with a sensor-to-ground transmittance, i.e.,

$$1/C_{jk} = \exp(-\tau_{jk}) \tag{4}$$

where the τ_{jk} are optical depths.

The τ_{jk} are extrapolated to the IR using an Angstrom Law proportionality ($\tau \sim \lambda^{-N}$, where N ≈1.5 for a typical aerosol), and the IR gains are computed from the result using Eq. (4).

The IR offsets, which are due to scattering, are assumed to be proportional to the atmospheric absorption, i.e.,

$$B_{jk} \sim 1 - 1/C_{jk} \tag{5}$$

The constant of proportionality in (5) is determined from the longest wavelength visible band, which is typically near 0.65 μm.

1.4 Application to synthetic wide-angle hyperspectral data

Here we demonstrate the wide-angle image destriping method on synthetic imagery, which provides the advantage of a "ground truth" surface. The images were generated using our first-principles MCScene code starting from a reflectance image of Davis, CA retrieved from HyMap hyperspectral data.[9] MCScene[1,10] is a Monte Carlo photon propagation model that is based on MODTRAN®[11] optical and atmospheric properties. The calculation used 1000 Monte Carlo "photons" per pixel per band together with noise removal post-processing.[12] The atmosphere is the Mid-Latitude Summer model with added haze, given by the rural aerosol model with a visibility of 16 km (vertical optical depth = 0.5 at 550 nm). The viewing geometry is shown in Figure 2. The sensor is at 2 km altitude, the off-nadir angle along the center axis is 45 deg, and the sun is at 45 deg from zenith. Images were generated for two different solar azimuth angles, 73 deg and 180 deg from the LOS. For the purpose of adjacency effect modeling the surface surrounding the original HyMap swath was modeled with the scene-average spectrum. The full MCScene image contains 301x301 pixels of IFOV = 2 mrad, for a 34.5 deg wide FOV in each direction. The 180 deg azimuth image shown in Figure 1 has been trimmed to mask the surface outside the HyMap swath.

The MCScene output, in units of apparent reflectance, was converted to nominal reflectance units using the empirical, in-scene QUAC[7] method. QUAC can accept radiance, apparent reflectance, or true reflectance data as input, and the results are quite insensitive to the particular form of the data. It should be noted that since all of these data forms are linearly related, they provide identical images when displayed with an auto-scaling method such as ENVI's "linear 2%" display. However, since QUAC is not exact even under the best of conditions, the QUAC-processed, destriped spectra will not quite match the original reflectance spectra input to MCScene. Therefore for a fairer assessment of the destriped spectra we compare them with the input reflectances after processing with QUAC.

Six IR reference bands, at 0.78, 0.85, 1.02, 1.23, 1.65 and 2.2 μm, were used for the gain determination step. Trials with images rebinned to the Landsat-7 response functions, which correspond to the second, fifth and sixth bands, indicated that reasonable results can also be obtained using only those three bands (i.e., $N = 3$). Results of similar quality were obtained for the MCScene images at both solar azimuth angles; the 180 deg results, which required a larger destriping correction, are presented here.

True color renderings of the results are shown in Figure 5, which compares the reflectance images with and without destriping to the input reflectance image. Nearly all of the additional haze contaminating the top of the image is removed by the destriping, making the contrast more consistent and improving the agreement with the true surface reflectance.

Spectral comparisons are shown in Figure 6 for a typical selection of pixels near the top of the image. While the destriping algorithm cannot remove the Monte Carlo "photon" noise from the MCScene calculations, otherwise it greatly improves the agreement with the input surface reflectances. The results for the vegetation and dark pixels at short wavelengths confirm that the bulk of the additional haze scattering at the top of the image is removed by the destriping process. The similar "before" and "after" results for the building indicate that, for bright pixels, the haze subtraction is counterbalanced by a gain boost, which compensates for the additional haze absorption.

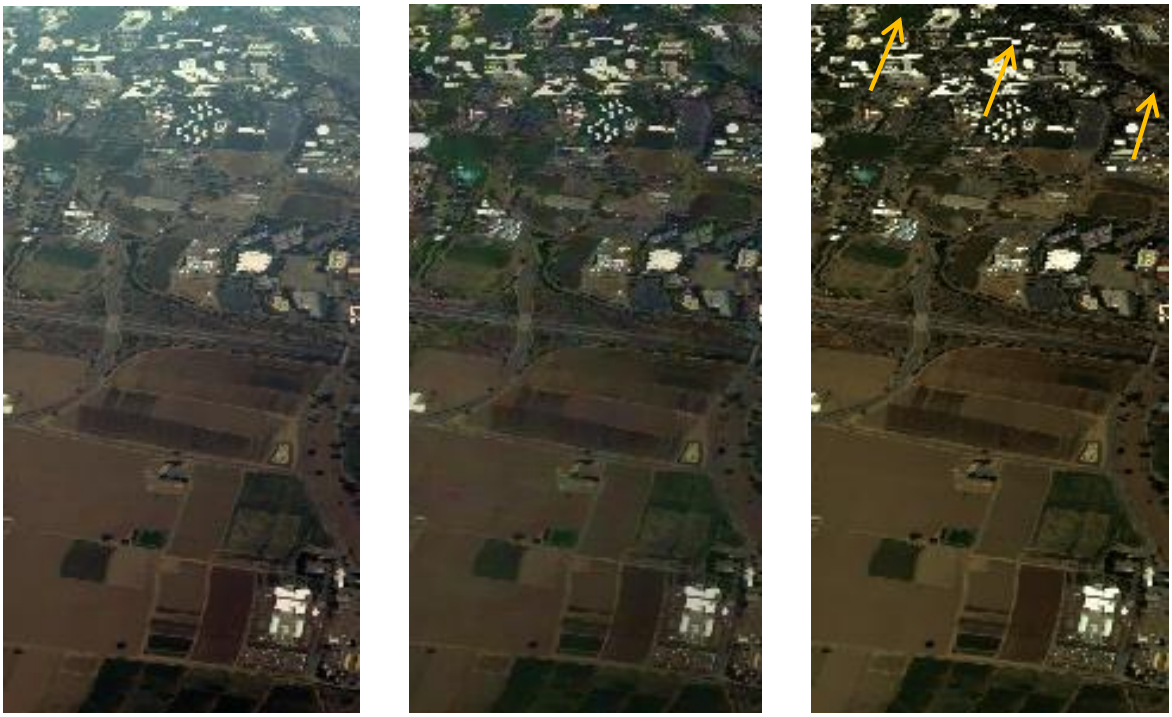

Figure 5. Comparison of Davis, CA images (ENVI "2% linear" rendering). From left to right, original apparent reflectance from Figure 2, destriped result, and true surface reflectance. Arrows show locations of the Figure 6 selected pixels.

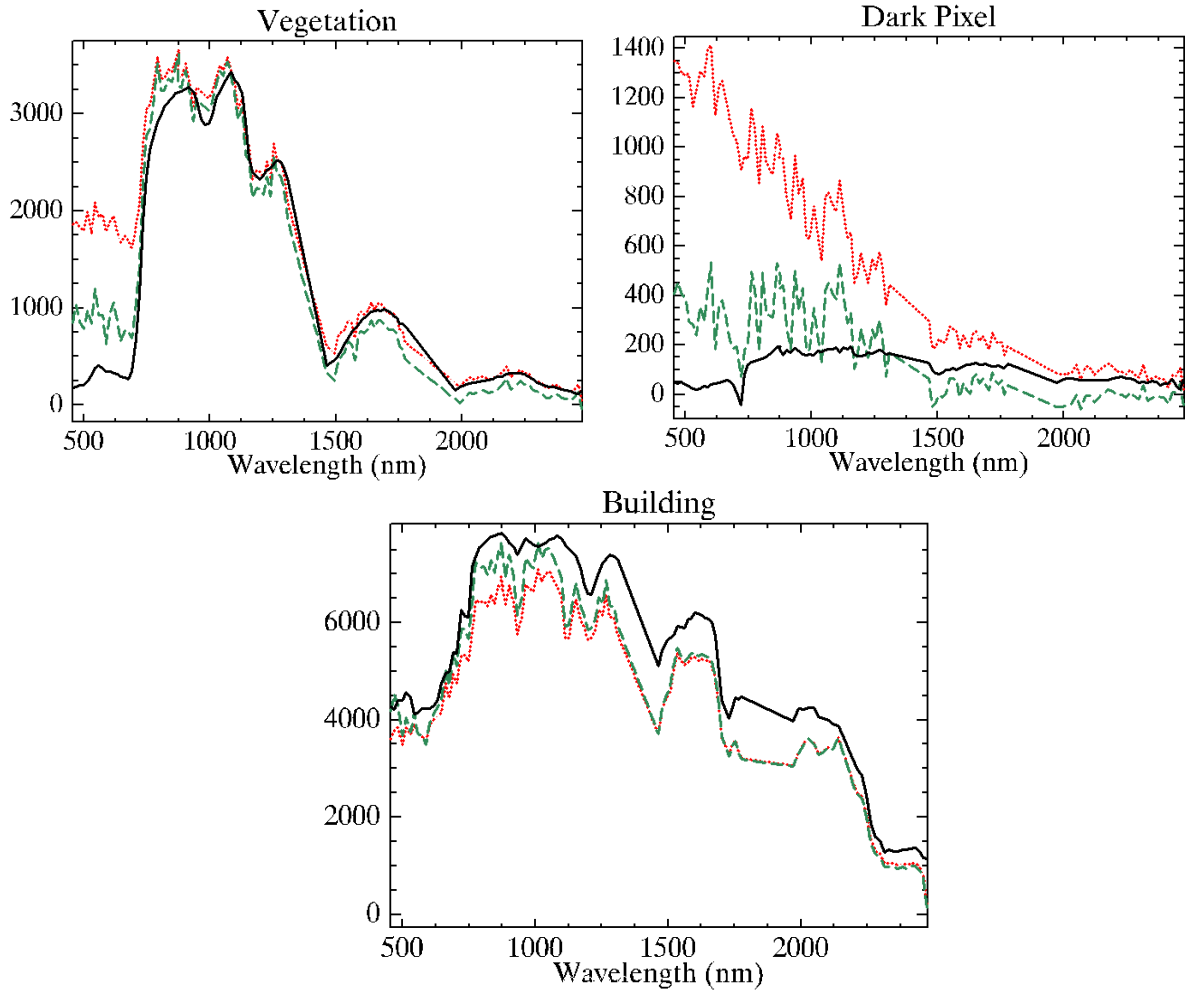

Figure 6. Reflectance spectra for selected Davis scene pixels near the top of the image. Y-axis is reflectance x10000. Red dotted curves = QUAC-processed MCScene image (no destriping); green dashed curves = result after destriping; black solid curves = QUAC-processed true reflectance.

2. CONCLUSIONS

Initial tests of the spectral image destriping approach described in this paper indicate that variants of the method can mitigate a wide variety of artifacts, including broad striping from viewing geometry variation and spectral "smile," which is very challenging for other algorithms. The method may be especially valuable for imagery in the thermal infrared, where detector arrays tend to be less well behaved than at shorter wavelengths. We plan to conduct further work to optimize the model dimensionality selection and to more extensively test and evaluate the method with a wide variety of data.

3. ACKNOWLEDGEMENTS

We greatly appreciate the contributions of G. Boer and A. Sanders of the National Geospatial-Intelligence Agency and A. Ifarraguerri of Science Applications International Corp. (SAIC). This work was funded under SAIC subcontract No. P010080877 and Spectral Sciences, Inc. IR&D.

REFERENCES

[1] Richtsmeier, S.C., A. Berk., S.M. Adler-Golden, and L.S, Bernstein, "A 3D Radiative-Transfer Hyperspectral Image Simulator for Algorithm Validation," Proc. ISSSR 2001, Quebec City, Canada (2001).

[2] Carfantan, H. and J. Idier, "Statistical Linear Destriping of Satellite-Based Pushbroom-Type Images," Trans. Geosci. Remote Sens. 48 (4), pp. 1860-1871 (2010).

[3] Kruse, F. A., "Use of Airborne Imaging Spectrometer data to map minerals associated with hydrothermally altered rocks in the northern Grapevine Mountains," Nevada and California: Remote Sensing of Environment, v. 24, no. 1, pp. 31-51 (1988).

[4] Van Mol, B. and K. Ruddick, "The Compact High Resolution Imaging Spectrometer (CHRIS): the future of hyperspectral satellite sensors. Imagery of Oostende coastal and inland waters," Proc. of the Airborne Imaging Spectroscopy Workshop, Brugge (2004).

[5] Sun, L., R. Neville, K, Staenz, and P. White, "Automatic destriping of Hyperion imagery based on spectral moment matching," Can. J. Remote Sens., vol. 34, pp. S68–S81, Suppl. 1 (2008).

[6] Smith, G.M. and E.J., Milton, "The use of the empirical line method to calibrate remotely sensed data to reflectance," Int. J. Remote Sensing, 20, 13, pp. 26563-2662 (1999).

[7] Bernstein, L.S., S.M. Adler-Golden, R.L. Sundberg, and A.J. Ratkowski, "Improved reflectance retrieval from hyper- and multispectral imagery without prior scene or sensor information," Proc. SPIE Vol. 6362, Remote Sensing of Clouds and the Atmosphere XI, 63622P (2006).

[8] Perkins, T., S.M. Adler-Golden, M.W .Matthew, A. Berk, L.S. Bernstein, J. Lee, and M. Fox, "Speed and accuracy improvements in FLAASH® atmospheric correction of hyperspectral imagery," Opt. Eng. 51(11), 111707 doi:10.1117/1.OE.51.11.111707 (2012).

[9] Rochford, P.A., P.K. Acharya, S.M. Adler-Golden, A. Berk, L.S. Bernstein, M.W. Matthew, S.C. Richtsmeier, S. Gulick, Jr., and J. Slusser, "Validation and Refinement of Hyperspectral/Multispectral Atmospheric Compensation Using Shadowband Radiometers," IEEE Transactions of Geoscience and Remote Sensing, Vol. 43, No. 12, (2005).

[10] Richtsmeier, S., R. Sundberg, "Recent Advances in the Simulation of Partly Cloudy Scenes," Proc. of SPIE 2010, Europe (Toulouse), (2010).

[11] Berk, A., G.P. Anderson, P.K. Acharya, *et al*, "MODTRAN®5: 2006 update," Proc. SPIE Int. Soc. Opt. Eng. 6233, 62331F (2006).

[12] Adler-Golden, S.M., D.C. Robertson, S.C. Richtsmeier, and A.J. Ratkowski, "Cloud Effects in Hyperspectral Imagery from First-Principles Scene Simulations," SPIE, Algorithms and Technologies for Multispectral, Hyperspectral, and Ultraspectral Imagery XV, Vol. 7334 (2009).